Experimental investigation and fast two-dimensional self-consistent kinetic modeling of a low-pressure inductively coupled rf discharge

U. Kortshagen,[1] I. Pukropski,[1] and L. D. Tsendin[2]

[1] Ruhr-Universität Bochum, D-44780 Bochum, Germany

[2] St. Petersburg State Technical University, 195251 St. Petersburg, Russia

(Received 16 January 1995)

We present a fast self-consistent kinetic model for an inductively coupled low-pressure rf discharge. The electron kinetics in it is described in terms of a nonlocal electron distribution function, which depends only on the total electron energy (kinetic plus potential one in the stationary electric field). In this case, the Boltzmann equation reduces to a one-dimensional ordinary differential equation in total energy. The complete model also includes the equations for ion motion, for the rf oscillatory induction field, for the external circuit, and the quasineutrality condition. It allows us to express all the plasma characteristics — the electron distribution function, the plasma density profile, the profiles of the stationary and of the oscillatory electric fields, the profiles of the excitation and ionization rates, etc.—in terms of the external characteristics—the chamber geometry, gas pressure, frequency, and the current in the primary coil. The theoretical predictions are compared to experimental results. An experimental investigation has been performed on an inductively coupled low-pressure rf discharge in Ar at 13.56 MHz over a wide range of input powers at gas pressures from 1 to 12 Pa. A satisfactory agreement with the experiment and qualitative interpretation of the observed phenomena is achieved.

PACS number(s): 52.80.Pi, 51.50.+v, 52.40.Hf, 52.50.Dg

I. INTRODUCTION

The problem of gas discharge modeling has attracted considerable and increasing interest. It is connected to the wide and growing number of applications of various gas discharge devices in such fields as surface processing, microtechnology, plasmachemistry, light sources, ecology, etc. For the construction and optimization of such devices effective methods of engineering calculations are necessary [1–4].

The current work on the numerical modeling of various types of discharges is of great scope. A number of impressive results have been achieved in the past (see, for example, [5–19]). However, the main efforts in these investigations were often concentrated on the maximal account of the physical processes involved and on the development of maximally accurate and fast-convergent numerical methods. In many of these studies computationally expensive methods such as Monte Carlo schemes or time-dependent fluid models coupled to the self-consistent solution of the Poisson equation for the slowly varying potential fields have been used. In any case, the great distinction between characteristic spatial and temporal scales, which is typical for plasma problems, makes such calculations very complicated and time consuming and demands computers of high computational power. The detailed analysis of the underlying physical principles by variation of various parameters is thus frequently not possible. Nevertheless, even the quantitative accuracy of these methods may be questionable, for instance, if they are based on inaccurate sets of cross sections. This circumstance may be one of the main reasons for the fact that up to now plasma technologies have been developed (and existing ones optimized) mainly empirically. In this respect

we are far from the ideal situation where the strategy of technological development is chosen mainly by means of plasma modeling and only relatively small numbers of experiments are necessary to check the chosen approach.

On the other hand, the physical understanding of complex, self-organizing, many-parameter systems such as gas discharges is impossible without numerical experiments, which are oriented towards obtaining physical understanding of the underlying processes. Such calculations do not demand high accuracy and can be performed for maximally simplified or, even preferably, model systems. Their main aims consist of the understanding of the dependencies of the plasma properties from the external parameters, in the finding of scaling laws, and in the development of effective approximations. For this purpose, it is extremely desirable to stimulate the development of simple and flexible methods for the modeling of gas discharges. The possibility of a serious reduction of the computational work and of the creation of such efficient models lies, we believe, in the optimal synthesis of numerical and analytical approaches. By performing analytically some sort of averaging over fast plasma motions, by introducing from the beginning the division of the whole discharge volume into the quasineutral plasma and space charge sheaths, and by replacing the sheaths by some effective boundary conditions, etc., it is often possible to eliminate from the beginning the fast time scales and the sharp transition layers of steep variation of the plasma parameters, which are the source of a great part of the computational problems.

A considerable step in this direction was made when the so-called nonlocal approach [20,21] to the solution of the electron Boltzmann equation in spatially inhomogeneous plasma was formulated. At relatively low pres-

sures the spatial motion of the plasma electrons, which are trapped by the space-charge field, is fast compared to considerable changes of their energy. It was demonstrated that the Boltzmann equation, which for the case of small anisotropy of the electron distribution reduces to a second order partial differential equation with shifted arguments, can be averaged over these fast spatial motions. It can be reduced to an ordinary differential equation, if the total (kinetic plus potential) electron energy is used as an argument of the distribution function, instead of the standardly used kinetic energy. This fact was checked in numerous experiments [22–25]. The efficiency of this approach was demonstrated in the self-consistent modeling of the dc positive column [26,27], the anode [28,29], and cathode [30] regions, and in the accurate description of the electron kinetics in inductively coupled rf discharges (RFI) [31,32]. In the capacitively coupled rf (RFC) discharge the computation time could be reduced by orders of magnitude by averaging over the fast electron motions in order to obtain the equations on the slow ion time scale (or even the stationary one) [34–36]. This procedure was combined with the nonlocal approach for the description of low pressure RFC discharges [37,33].

In this paper we describe a model, which is based on the above ideas, for the inductively coupled low-pressure rf discharge. This discharge concept is of growing practical interest especially in the field of semiconductor etching and deposition [1,38–40]. Stable, relatively high-density ($\sim 10^{11} - 10^{13}$ cm^{-3} [3,38,41]) plasmas can be created in RFI discharges at pressures of the order of 10 mTorr with a low sheath bias voltage. The ion flux to the substrate is practically monoenergetic and highly anisotropic. The ion energies are significantly smaller than in the RFC discharge. Accordingly, the surface damage can be considerably reduced. The low operating pressures and the fact that the dimensions of the discharge chamber are comparable to the energy relaxation length of the electrons makes the nonlocal approach applicable with high accuracy. It was convincingly demonstrated in [25,32]. Since the sheath voltages in these discharges are of the order of the electron temperature, secondary electrons are negligible and the well-known two term approximation for small anisotropy of the EDF can be used instead of solving the complete Boltzmann equation or using straightforward Monte Carlo methods in a three-dimensional velocity space. However, the principally two-dimensional character of the inductive rf field implies the necessity of a two-dimensional formulation of the whole problem.

An impressive attempt of straightforward modeling of such discharges was made in [11,12]. The model consisted of an electromagnetic module for calculating the rf fields, a Monte Carlo electron simulation, a hydrodynamic description of ions and neutrals, the Poisson equation for the potential electric field, and even a plasmachemical module. Concrete reactor details such as a powered wafer electrode and a stationary multipole magnetic field were accounted for. This program gave rather reasonable results but the calculations were very time consuming. On the other hand, several crude assumptions could not be avoided, such as the assumption of a field-independent ion mobility or imposing a boundary condition for the inductive field at the top dielectric plate without accounting for the fields, which are produced by the currents in the other metallic walls. However, the most surprising result of [11,12] involves the strong correlation between the positions of the maximal energy input and the maximal excitation and ionization rates.

Such a correlation seems quite natural in the fluid approach (e.g., [42]), as can be seen from the consideration of the electron energy balance equation. The main terms in the energy balance are the energy input by Joule heating, the energy losses by excitation and ionization and thermal conduction, while the diffusion cooling is usually negligible [43]. Without thermal conductivity the maxima of energy input and energy losses would coincide. The thermal conductivity, however, is able only to reduce the relative height of the energy loss density maximum with respect to the relative height of the power deposition maximum, but it is incapable of shifting its position considerably. The energy deposition and losses are thus strongly spatially correlated in fluid approaches, as was observed in [42]. Under low-pressure conditions, however, the electron energy relaxation length

$$\lambda_\epsilon = \sqrt{\lambda \lambda^*} \qquad (1)$$

may exceed the chamber dimensions (λ is the transport mean free path and λ^* the mean free path for inelastic collisions). In this case, the total electron energy (kinetic plus potential in the quasistationary space-charge electric field) is conserved during electron spatial motion. It means that independent of the precise position, where any given electron gains its energy, it will lose it with the maximal probability in the place where its kinetic energy (at constant total energy) is maximal, namely in the maximum of the plasma density close to the geometric center of the discharge. This effect was observed in numerous experiments in dc, RFI, and in RFC discharges. With decreasing pressure the maximum luminosity in rf discharges shifts from the periphery, where the energy input is concentrated (skin effect in RFI discharges, low conductivity in RFC discharges), towards the chamber center [44,31]. The fluid approach is not capable of accounting for these nonlocal effects, since it is based on the unified description of electrons: the EDF in any place is characterized by three parameters — density, velocity, and mean energy. It implies that during its motion a given electron "knows" about all others in this place. Since at low pressures the spatial displacement of electrons occurs faster than their energy relaxation, this assumption is physically inconsistent.

In this paper we therefore present a simple model, which is based on the kinetic description of the electrons. After introducing briefly our experimental setup in Sec. II, a detailed description of the kinetic, two-dimensional model is presented in Sec. III. A comparison and discussion of experimental and theoretical results is given in Sec. IV, while the main results and conclusions are summarized in Sec. V.

II. EXPERIMENTAL SETUP

In the present experiment (for details see [25]) we restricted ourselves to the case of a purely inductively coupled rf discharge at a frequency of 13.56 MHz in argon at pressures from 0.9 to 12 Pa.

The experimental setup used in this investigation is sketched in Fig. 1. The discharge vessel had a height of L= 6 cm and a radius of R = 7.5 cm. The side wall and the top plate of the vessel were made of glass and the bottom plate was constructed of aluminum. The rf field is induced via a spiral coil with four turns of a bent copper tube. The rf power was generated by a power amplifier with a maximum output power of 1000 W. However, only much smaller rf powers have been applied due to the considerable thermal load of the coupling structure. The rf power was coupled to the coil via a matching network. The output power of the amplifier and the matching of the discharge impedance to the output impedance of the amplifier were monitored via a standing wave ratio meter. Of course, the measured output power was (much) larger than the power absorbed by the plasma. A considerable part of the rf power may have been dissipated in the matching network and the feeding cables. To determine the power absorbed by the plasma as well as the reactive power of the coil-plasma system, the rf current and voltage had to be measured. These measurements were performed close to the coil (after the matching network) using a current transformer and a capacitive voltage divider. The capacitive coupling, which is usually dominating at low input power levels, was strongly reduced by a Faraday shield, which enclosed the whole induction coil. Its bottom plate was a radially slit copper plate, which allowed the magnetic field to penetrate into the plasma volume but which screened the electrostatic field. The reduction of the capacitive power transfer was necessary in order to reduce the disturbance of the probe measurements caused by rf modulation of the plasma potential. However, the grounded screen also introduced

additional stray capacitances, so that the rf current may partially have flown through these capacitances rather than through the induction coil. The whole system was evacuated by a turbo molecular pump to a basic pressure of less than 10^{-6} mbar. During the active plasma phase the system was operated with a constant gas flow. In this case, a rotary pump with small pumping power was used.

For the measurements of the EDF a pulsed probe technique was used [45,46]. The compensation of the remaining rf fluctuations of the plasma potential was achieved by means of passive compensation [47,46]. Two coils for the fundamental frequency of 13.56 MHz and a coil for the harmonic frequency at 27.12 MHz were mounted within a distance of 3 cm from the probe tip in order to provide a high rf impedance between the probe sheath's impedance and the ground. A metallic cylinder was coupled capacitively to the probe in order to increase the plasma-probe capacitance and thus to diminish the probe sheath impedance [48,49,46]. During the experimental work it turned out that particularly at high plasma densities the blocking coils are superfluous [50]. In this case, the remaining capacitive coupling was obviously strongly reduced so that no considerable rf distortions of the probe measurements appeared. The probe was introduced via a flange from the side wall and could be moved in the radial direction. By the use of a curved probe holder, it was also possible to perform axially resolved measurements by rotation of the probe. The grounded metallic bottom plate acted as the counterelectrode for the probe circuit. By initially using an additional sensing probe, it was determined that the floating (and thus hopefully also the plasma) potential was not significantly affected by the current drain of the measuring probe or any sources of fluctuations (e.g., low-frequency fluctuations due to the rf power generator).

III. THE KINETIC TWO-DIMENSIONAL DISCHARGE MODEL

A. Solution of the Boltzmann equation

In the investigated range of parameters, as can be seen from experiment and the presented calculations, the electron energies have not considerably exceeded 20 eV. It implies that the electron mean free path λ at all energies of interest (with the exception of those energies close to the Ramsauer minimum) and at all investigated pressures was small compared to the chamber dimensions.

A complicated problem involves the interaction of the electrons with the strongly inhomogeneous rf field. Its characteristic scale decreases with increasing plasma density from the chamber dimension $\min[R, L]$ to the skin layer thickness δ due to the skin effect (see below, Sec. III C). In our case, spatially propagating waves and the associated resonance plasma heating mechanism [51,52] are absent. As was pointed out in [53], the remaining problem is reduced to the theory of the normal and anomalous skin effect (see, for example, [54]). The main result can be formulated roughly as follows. If $\omega < \nu$ and $\lambda < \delta$, the normal skin effect occurs with a station-
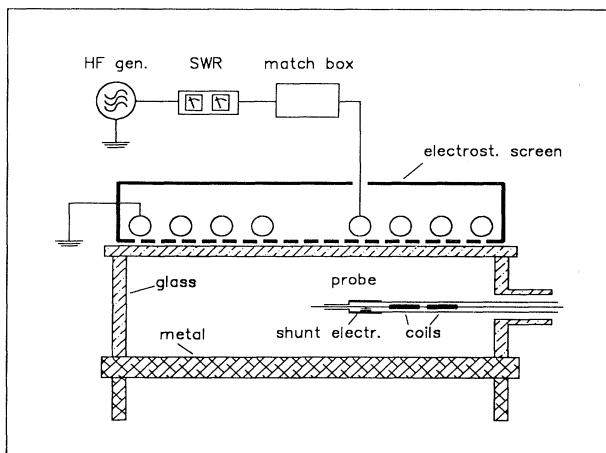

FIG. 1. Experimental setup of the inductively coupled plasma. The height of the discharge vessel is 6 cm, its diameter 15 cm.

ary conductivity. The transition to the anomalous one takes place at high frequencies $\omega > \nu$, if the skin layer thickness satisfies $\delta < \lambda\nu/\omega, \lambda$. In this case the spatial dispersion is important and the inhomogeneity of the rf field has to be taken into account. Here, we shall restrict ourselves to the case

$$\lambda < L, R, \delta . \tag{2}$$

In this situation the conventional two-term expansion for the EDF is applicable:

$$F(\mathbf{r}, \mathbf{v}, t) = F_0(\mathbf{r}, v, t) + \frac{\mathbf{v}}{v} \cdot \mathbf{F_1}(\mathbf{r}, v, t) . \tag{3}$$

If condition (2) holds, it is possible to neglect the collisionless electron heating mechanism due to an anomalous skin effect [53,55].

Only at the highest values of the pressures considered is the maximal value of the inelastic collision frequency ν^*, which corresponds to the maximal inverse electron energy relaxation time over the whole EDF, comparable to the rf angular frequency ω. It means that the isotropic part of the EDF F_0 can be considered time independent [56]. (Very similar ideas with respect to the nonlocal electron kinetics, but without solution of the total self-consistent problem, were developed in [31,57].)

In the presence of the oscillatory solenoidal rf field $\mathbf{E}(\mathbf{r}, t) = \mathbf{E}_0(\mathbf{r}) \exp i\omega t$ and of the (quasi)stationary potential electric fields, the vector part of the EDF $\mathbf{F_1}(\mathbf{r}, v, t)$ splits naturally into the oscillatory part

$$\tilde{\mathbf{F}}_1 = \frac{e\mathbf{E}(\mathbf{r}, t)}{m(i\omega + \nu)} \frac{\partial F_0}{\partial v} , \tag{4}$$

and the (quasi) stationary part

$$\mathbf{F_1} = -\frac{v}{\nu}\nabla_\mathbf{r} F_0 + \frac{e}{m\nu}\nabla_\mathbf{r}\Phi\frac{\partial F_0}{\partial v} . \tag{5}$$

The fulfillment of (2) enables us to neglect the spatial dispersion terms in Eq. (4) even if $\omega > \nu$. This case is equivalent to the skin effect in the infrared frequency region (paragraph 87 in [54], cf. [53]). In Eqs. (4) and (5) $\Phi(\mathbf{r})$ denotes the stationary potential of the space-charge electric field (it can also be time dependent on the slow time scale of the ion motion), and $\nu(v)$ denotes the transport frequency for electron atom collisions. Substituting Eqs. (4) and (5) into the equation for the isotropic EDF $F_0(\mathbf{r}, v)$ and averaging it over the rf period (keeping in mind that F_0 is time independent), we obtain

$$-\nabla_\mathbf{r} \cdot \left(\frac{v^2}{3\nu}\nabla_\mathbf{r} F_0\right) + \frac{ve}{3m}\nabla_\mathbf{r} \cdot \left(\frac{\nabla_\mathbf{r}\Phi}{\nu}\frac{\partial F_0}{\partial v}\right) - \frac{e}{3mv^2}\frac{\partial}{\partial v}\left[-\frac{v^3}{\nu}\nabla_\mathbf{r}\Phi \cdot \nabla_\mathbf{r} F_0\right.$$
$$\left. + \frac{ev^2}{m\nu}\left((\nabla_\mathbf{r}\Phi)^2 + \frac{E^2}{2}\frac{\nu^2}{\nu^2 + \omega^2}\right)\frac{\partial F_0}{\partial v}\right] = C_0(F_0) , \tag{6}$$

where $C_0(F_0) = C_{0,elast} + C_{0,exc} + C_{0,ee}$,

$$C_{0,elast} = \frac{1}{2v^2}\frac{\partial}{\partial v}\left[v^3\kappa\nu\left(F_0 + \frac{kT_g}{mv}\frac{\partial F_0}{\partial v}\right)\right] ,$$
$$C_{0,exc} = -\sum_k \left(\nu^k(v)F_0(\mathbf{r}, v) - \frac{v'}{v}\nu^k(v')F_0(\mathbf{r}, v')\right) . \tag{7}$$

$C_{(0,elast)}$ and $C_{(0,exc)}$ are the collision terms for elastic and inelastic electron-atom collisions, respectively, $v' = \sqrt{v^2 + u_k/(2m)}$, u is the kinetic energy of electrons, $\nu^k(u)$ and u_k are the excitation frequency and energy of the kth atomic level, respectively, and $\kappa = 2m/M_a$. The expressions for the collision integral of the electron-electron collisions $C_{0,ee}$ can be found, for example, in [58]. Introducing, according to [20,21], the total energy $\epsilon = u + e\Phi$ and $\mathbf{r}$ as variables (instead of $\{\mathbf{r}, v\}$), it is possible to reduce Eq. (6) to a diffusion equation in space and total energy,

$$-\frac{1}{3v}\nabla_\mathbf{r} \cdot \left(\frac{v^3}{\nu}\nabla_\mathbf{r} F_0\right) - \frac{1}{3v}\frac{\partial}{\partial\varepsilon}\left[\frac{v^3}{\nu}\left(\frac{E_0^2}{2}\frac{\nu^2}{\nu^2 + \omega^2}\right)\frac{\partial F_0}{\partial\varepsilon}\right] = C_0[F_0(\varepsilon)] , \tag{8}$$

where $F_0 = F_0(\epsilon, \mathbf{r})$. The spatial and the energy diffusion coefficients are equal to

$$D = \frac{v^2}{3\nu} , \tag{9}$$

$$D_\epsilon = \frac{(eE_0)^2 v^2 \nu}{6(\omega^2 + \nu^2)} = \frac{(eE_{eff}[\mathbf{r}, u(\epsilon, \mathbf{r})]\lambda)^2 \nu}{3} . \tag{10}$$

Instead of Eq. (5) we obtain

$$\mathbf{F_1}(\epsilon, \mathbf{r}) = -\frac{v}{\nu}\nabla_\mathbf{r} F_0(\epsilon, \mathbf{r}) . \tag{11}$$

It is necessary to bear in mind that the spatial derivatives in Eqs. (8) and (11) have to be calculated at the constant ϵ, instead of v, and that the coefficients here are $(\epsilon, \mathbf{r})$ dependent due to the dependencies on $v(\epsilon, \mathbf{r})$
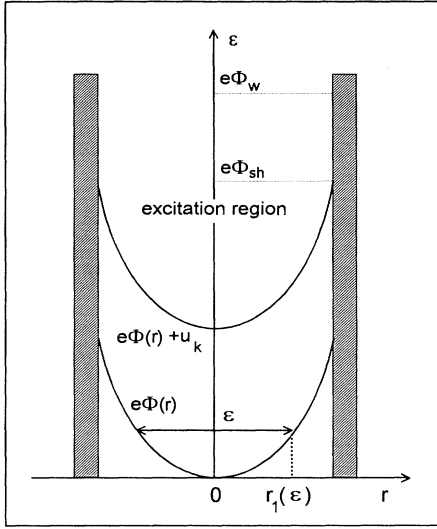
FIG. 2. The accessible domain for electrons in the frame coordinate–total energy. $r_1(\varepsilon)$ denotes the turning point for electrons with the total energy ε.

and $\mathbf{E}_0(\mathbf{r})$. For the electrons, which are trapped by the space-charge field, Eq. (8) can be integrated over the part $V_{ac}(\epsilon)$ of the total discharge volume V_0, which is accessible for an electron with a given total energy ϵ (Fig. 2). The accessible volume is defined by

$$u(\mathbf{r}) \geq 0 \quad \text{or} \quad \varepsilon \geq \Phi(\mathbf{r}) , \quad \forall \mathbf{r} \text{ in } V_{ac} , \qquad (12)$$

and its boundary $\mathbf{r}_1(\epsilon)$ is given by

$$u(\mathbf{r}_1(\epsilon)) = 0 . \qquad (13)$$

The first term in the left-hand side of Eq. (8), which is of the highest order in the ratio $[\lambda_\epsilon/(R,L)]$, cancels identically during the spatial averaging of the kinetic equation (8). The nonlocality condition

$$\lambda_\epsilon \gg R, L \qquad (14)$$

results in an insignificant dependence of F_0 on $\mathbf{r}$ so that in the remaining terms of the Boltzmann equation $F_0(\epsilon, \mathbf{r})$ can be replaced by its spatially uniform main part $F_0^{(0)}(\epsilon)$ [20,21]. One obtains

$$-\frac{d}{d\varepsilon}\overline{u^{1/2}D_\epsilon}(\varepsilon)\frac{dF_0^{(0)}}{d\varepsilon} = \overline{u^{1/2}C_0[F_0^{(0)}(\varepsilon)]} , \qquad (15)$$

where the spatially averaged energy diffusion coefficient (times $u^{1/2}$)

$$\overline{u^{1/2}D_\epsilon}(\varepsilon) = \frac{1}{V_0}\frac{2e^2}{3m}\int_{V_{ac}} \frac{u^{3/2}(\mathbf{r})}{\nu(u(\mathbf{r}))}E_{eff}^2(\mathbf{r}, u(\mathbf{r}))\,dV \qquad (16)$$

has been introduced. On the right-hand side the following terms are included:

$$\overline{u^{1/2}C_{0,ex}} = -\sum_k [\overline{u^{1/2}\nu^k}(\varepsilon)F_0^{(0)}(\varepsilon)$$
$$-\overline{u^{1/2}\nu^k}(\varepsilon + u^k)F_0^{(0)}(\varepsilon + u^k)] \qquad (17)$$

with

$$\overline{u^{1/2}\nu^k}(\varepsilon) = \frac{1}{V_0}\int_{u(\mathbf{r}) \geq u^k} \nu^k(u(\mathbf{r}))u^{1/2}(\mathbf{r})\,dV . \qquad (18)$$

The averaging is performed over the region where the kth excitation process is possible. This region is sketched in Fig. 2 as the "excitation region." The electron-electron, superelastic, and ionization collision terms can be expressed in an analogous manner. The elastic collision term is simplified by neglecting the recoil term, since the gas temperature kT_g is usually much smaller than the electron temperature. For this case one obtains

$$\overline{u^{1/2}C_{0,el}} = \frac{d}{d\varepsilon}[\bar{V}_\epsilon F_0^{(0)}(\varepsilon)] ,$$
$$\bar{V}_\epsilon = \frac{1}{V_0}\int_{V_{ac}} \kappa\nu_m(u(\mathbf{r}))u^{3/2}(\mathbf{r})\,dV . \qquad (19)$$

In this nonlocal approximation the extremely complicated problem of the solution of a three-dimensional partial differential equation (8) is reduced to the standard one-dimensional problem of solving Eq. (15). Although one unique EDF of total energy results from the solution of (15), the spatial information is still fully retained in it, provided the profile of the space-charge potential $\Phi(\mathbf{r})$ is known. The EDF of kinetic energy in any given point of the discharge volume $F_0(u, \mathbf{r})$ can be found from the EDF $F_0^{(0)}(\epsilon)$ by a simple back substitution $u = \epsilon - e\Phi(\mathbf{r})$:

$$F_0(u, \mathbf{r}) = F_0^{(0)}[\varepsilon = u + e\Phi(\mathbf{r})] . \qquad (20)$$

The meaning of this equation is that the EDF of the kinetic energy at a given position $\mathbf{r}$ is obtained from the EDF of the total energy by removing the low-energy part of the electron spectrum, which corresponds to the electrons with a total energy less than the potential energy at the position $\mathbf{r}$. These electrons simply are incapable of reaching the point of observation and they are trapped by the space-charge field in the inner plasma region.

The ideology of the procedure of the spatial averaging of the Boltzmann equation is similar to the standard procedure of its temporal averaging, which was used to derive Eq. (6). In both cases the fast temporal or spatial variation of the fields results, due to the EDF's inertia, in a feeble dependence of the EDF on the temporal or on the spatial coordinates, which can be neglected in the first approximation.

A more complicated situation arises with the more energetic electrons, which are capable of abandoning the discharge volume and to be absorbed by the walls. The EDF for these electrons (with $\epsilon > e\Phi_w$, where Φ_w is the wall potential) depends, strictly speaking, not only on ϵ but also on the coordinates and even on the velocity direction [59]. The form of the EDF in this energy region depends also substantially on the wall material. In the case of metal walls, the value of Φ_w is constant over

the whole wall surface. Over dielectric walls a profile of Φ_w arises, which is determined by the equality of the ion and electron fluxes at every point of the wall. In our calculations we accounted for this fact approximately by introducing an energy-dependent escape term into the right-hand side of Eq. (15)

$$C_{0,wall} \approx \frac{\varepsilon^{1/2} F_0^{(0)}(\epsilon)}{\tau_w(\epsilon)} . \tag{21}$$

The wall loss time $\tau_w(\epsilon) = 1/\nu_w$ is determined by the diffusion and by the probability that the velocity direction of a fast electron at the plasma-sheath boundary lies in the loss cone. If the first process dominates, the loss time is equal to the mean diffusion time τ_{diff} which is necessary for the electron to reach the plasma-sheath boundary:

$$\nu_{diff} = \frac{1}{\tau_{diff}} = \frac{D}{\Lambda^2} = \frac{\nu\lambda^2}{3\left(\frac{\pi^2}{L^2} + \frac{2.4^2}{R^2}\right)} , \tag{22}$$

where D is the electron diffusion coefficient (9) and Λ is the characteristic scale of the discharge. In the opposite case the mean escape frequency is equal to

$$\nu_s = \frac{1}{\tau_s} = v(\epsilon - e\Phi_{sh}) \frac{\delta\Omega(\epsilon)}{4\pi} \frac{S_0}{V_0} , \tag{23}$$

where $\delta\Omega(\epsilon)$ is the solid angle of the loss cone

$$\delta\Omega = 2\pi \left(1 - \sqrt{\frac{e(\Phi_w - \Phi_{sh})}{\varepsilon - e\Phi_{sh}}}\right) . \tag{24}$$

For the definition of Φ_w and Φ_{sh}, see Fig. 2. S_0 and V_0 are the surface area and the volume of the chamber, respectively. In the intermediate case, a simple interpolation gives

$$\nu_w = \frac{1}{\tau_w} = \frac{1}{\tau_{diff} + \tau_s} . \tag{25}$$

Since the whole consideration is performed for a typical electron, the wall loss frequency ν_w can also be considered as a cross section averaged characteristic.

Since the escape time (25) is determined by the free diffusion of the fast electrons, it is comparatively short and at $\epsilon > e\Phi_w$ the EDF decreases rapidly. On the other hand, in the stationary case the total ionization rate has to be equal to the total flux of the fast electrons to the wall. It means that in the nonlocal regime the wall potential $e\Phi_w$ has to be close to the effective ionization potential, which coincides with the real ionization potential, when direct ionization dominates, or it is close to the first excitation potential, if stepwise processes supply the main part of charged particles. If it were not so, the exponential decrease of the EDF, which is caused by the inelastic collisions as well as by the wall losses (25), makes it impossible to satisfy the ionization-wall loss balance.

The spatial dependence of the EDF tail at $\epsilon \gtrsim e\Phi_w$, which is due to the escape of the fast electrons to the chamber walls, and at $\epsilon \gtrsim u_1$ (the first excitation poten-

tial), which may result from the deviations from non-locality, was neglected in Eqs. (15) and (21). These mechanisms can produce some slight additional inhomogeneities in the spatial profiles of the ionization rate (see [57]), which will not be considered here.

If the profiles of the stationary potential $\Phi(\mathbf{r})$ and of the rf electric fields $\mathbf{E}(\mathbf{r},t)$ are given, the solution of Eq. (15) gives the EDF $F_0^{(0)}(\epsilon)$ in the whole discharge volume. It is determined up to an arbitrary numerical factor, which can be interpreted as the electron density in the chamber center n_0. The rates of all the processes, which are stimulated by the electrons, such as excitation, ionization, or the electron current to the chamber walls, etc., can be derived from $F_0^{(0)}(\epsilon)$. The density of the rf current and the complex conductivity of the plasma can also be expressed by means of Eq. (4) in terms of the same EDF:

$$\mathbf{j}(\mathbf{r},t) = -\frac{2e^2 \mathbf{E}(\mathbf{r},t)}{3m} \int_{e\Phi(\mathbf{r})}^{\infty} \frac{u^{3/2}}{\nu + i\omega} \frac{\partial F_0^{(0)}}{\partial\epsilon} d\epsilon$$

$$= \sigma(\mathbf{r})E(\mathbf{r},t) = (\Sigma_1 - i\Sigma_2)\mathbf{E}(\mathbf{r},t) , \tag{26}$$

where $\Sigma_2/\Sigma_1 \sim \omega/\nu$.

B. Ion motion and the potential profile

In practically the whole discharge volume the quasi-neutrality condition is fulfilled with a high accuracy. It means that we can use the expression for the electron density

$$n(\Phi(\mathbf{r})) = \int_{e\Phi(\mathbf{r})}^{\infty} F_0^{(0)}(\epsilon)[\epsilon - e\Phi(\mathbf{r})]^{1/2} d\epsilon \tag{27}$$

in the balance equation for the ion density (28), which can be treated as an equation for the potential profile $\Phi(\mathbf{r})$. Neglecting the thermal energy of the ions in comparison to that of the electrons as well as their inertia, the ion continuity and momentum equation can be combined to

$$\nabla_\mathbf{r} \cdot \left(\frac{e}{M_i \nu_{in}} n \nabla_\mathbf{r} \Phi\right) = n\nu_i(\mathbf{r}) . \tag{28}$$

Here, M_i is the ion mass and $\nu_i = \nu_i(\mathbf{r})$ denotes the spatially dependent mean ionization frequency, which is obtained as an integral over the EDF of kinetic energy: $F_0(u,r,z) = F_0^{(0)}[\epsilon - e\Phi(r,z)]$. The mean ion-neutral collision frequency ν_{in} is considered to be velocity dependent in the constant mean free path approximation:

$$\nu_{in} = \nu_{in,0}\left(1 + a\frac{M_a v^2}{kT_g}\right)^{1/2} \tag{29}$$

with $\nu_{in,0}$ the collision frequency at zero drift velocity, taken from [60], and $a = 0.182$ [61]. The boundary condition for this elliptic problem is that the Bohm criterion should be fulfilled in front of all walls. The Bohm criterion is formulated in the approximate form so that the potential drop in the plasma over the last ion mean free path before the wall has to be equal to $kT_e/2e$, i.e.,

$$e|\nabla_{\mathbf{r}}\Phi|\lambda_i = \frac{kT_e}{2} . \qquad (30)$$

The fulfillment of this boundary condition represents an eigenvalue problem for the rf electric field strength and thereby for the self-consistent rf coil current. On the discharge axis the symmetry leads to the boundary condition:

$$\left.\frac{\partial\Phi}{\partial r}\right|_{r=0} = 0 . \qquad (31)$$

For the low pressures considered in the present work the contribution of stepwise ionization should be negligible [62,63] so that only direct ionization has been taken into account on the right-hand side of Eq. (28).

The boundary condition (30) is applied at the plasma-sheath boundary. The thickness of the space-charge layer in the RFI discharges (in contrast to the RFC discharge) is negligible compared with the discharge dimensions. For our discharge conditions the ion mean free path λ_i was also always small with respect to R and L. Thus it follows that condition (30) can be imposed on the chamber walls. It is well known that in the collisional case the plasma density profile is not too sensitive to the boundary condition for the potential and is close to the profile, which corresponds to the zero plasma density at the chamber walls.

The question is how to define the electron temperature, which appears in the ion sound speed, for a non-Maxwellian EDF. In this work, the so-called screening temperature [64]

$$\frac{kT_e}{e} = -\left(\left.\frac{d\ln n_e}{d\Phi}\right|_{\Phi_{sh}}\right)^{-1} \qquad (32)$$

has been used. This definition relates the decrease of the electron density at the sheath boundary to a temperature. It is thus suited to describe the physical situation of the screening of the electrons by the sheath potential properly. For a Maxwellian EDF this definition yields the usual thermodynamic electron temperature.

The solution of Eqs. (28)–(31) results in a potential profile at the plasma-sheath boundary $\Phi_{sh}(\mathbf{r}_{wall})$. It should be noted that for an arbitrary profile of the rf energy input the Bohm criterion (30) is usually not satisfied at the chamber walls. By variation of the parameter n_0, which leads to the skin effect (see below), it is possible to satisfy (30). The reason lies in the fact that Eqs. (28)–(31) (in close analogy to the well-known Schottky problem of the ambipolar diffusion $D\Delta n + \nu_{in}n = 0$ with zero boundary conditions) also possesses the trivial solution. The nontrivial, nonoscillatory solution exists only for a unique choice of the parameter n_0 (it corresponds to the choice of ν_i in the Schottky case).

The value of the wall potential Φ_w (in the case of metal walls) can be found from the equation

$$\int_{V_0} n\nu_i d\mathbf{r} = \int_{V_0} d\mathbf{r} \int_{e\Phi(\mathbf{r})+u_{ion}}^{\infty} \nu_{ion}(u)u^{1/2}F_0^{(0)}(\epsilon)d\epsilon$$

$$= \int_{V_0} d\mathbf{r} \int_{e\Phi_w}^{\infty} \nu_w(\epsilon)u^{1/2}F_0^{(0)}(\epsilon)d\epsilon , \qquad (33)$$

with $\nu_w(\epsilon)$ from Eq. (25), and u_{ion} and ν_{ion} being the ionization energy and frequency, respectively. This equation expresses the fact that the total ionization rate has to be equal to the outflux of the fast electrons to the chamber walls. The difference between Φ_w and Φ_{sh} represents the potential difference over the space-charge sheath. It should be noted that it has nothing in common with the standardly used value of $(kT_e/2e)\ln(m/M_i)$ and that it is usually considerably smaller than the latter [65]. In our calculations we used the cross-section data of the elementary processes from [66].

C. Electrodynamics of the rf field and the external circuit

The spatial distribution of the rf field $\mathbf{E}$ can be found from the solution of Maxwell's equations. By combination of Faraday's induction law $\nabla \times \mathbf{E} = -\partial\mathbf{B}/\partial t$ and Ampère's law $\nabla \times \mathbf{H} = \partial\mathbf{D}/\partial t + \mathbf{j}$, one obtains the well-known wave equation. Since the inductive electric field due to the symmetry of the problem has only an azimuthal component, $\mathbf{E} = E\mathbf{e}_\vartheta$, one finds [67]

$$\nabla^2 E(r,z) = i\omega\mu_0 j(r,z)$$
$$= i\omega\mu_0\left[\sigma(r,z)E(r,z) + j_{coil}(r,z)\right] . \qquad (34)$$

Here, the electric vacuum displacement current has been neglected as compared to the conduction current. The index ϑ has been omitted at E and j. The current density in the plasma is given by Eq. (26), while the current density in the coil winding has to be specified as an external input parameter. The latter represents the source term in the above equation. From a numerical point of view, it is quite easy to implement an arbitrary coil configuration. However, for a more schematic discussion, the coil is approximated by a flat, homogeneous current distribution

$$j_{coil}(r,z) = \delta(z_{coil})\Theta(r - R_1)\Theta(R_2 - r)I_{coil}M . \qquad (35)$$

R_1 and R_2 are the inner and outer radii of the coil, respectively, Θ is the step function with $\Theta(x) = 0$ for $x < 0$ and $\Theta(x) = 1$ for $x \geq 0$, I_{coil} is the amplitude of the coil current, M is the number of coil windings per unit radius, and δ represents the Dirac function. According to our experimental setup, $R_1 = 0.5$ cm and $R_2 = 7.2$ cm have been chosen in the following.

Of course, the amplitude of the induced electric field is proportional to the current density in the coil. The boundary conditions for this problem are especially simple, if one assumes that the whole setup is surrounded by a cylindrical metallic chamber. In this case, the electric field, which is parallel to every wall, has to vanish due to the continuity of the tangential field component. The same boundary condition holds exactly on the coil axis. Hence, homogeneous boundary conditions apply for the whole range of integration $0 \leq r \leq R$, $0 \leq z \leq H$, where $H = 12$ cm is the height of the metallic screen of our model system:

$$E|_{walls} = 0 \quad \text{and} \quad E|_{axis} = 0 . \qquad (36)$$

Equations (34)–(36) represent a standard Dirichlet problem for the induction field E. Since the active and the reactive (real and imaginary) parts of the rf electric field are calculated, one can self-consistently determine the complex impedance of the complete system plasma-coil-discharge vessel. The knowledge of the impedance is important information for the design and construction of an RFI device. It forms the link between the electrotechnical design of the outer circuit and the kinetic properties of the plasma. The external circuit is only sensitive to the electromagnetic field, which is induced in the induction coil. The induced rf voltage is given by

$$U_{ind} = 2\pi M \int_{R_1}^{R_2} E(r, z_{coil})\, r\, dr \; . \tag{37}$$

The discharge impedance, i.e., the total impedance of the system coil-chamber plasma can thus be calculated as

$$Z = -\frac{U_{ind}}{I_{coil}} = \frac{2\pi M}{I_{coil}} \int_{R_1}^{R_2} E(r, z_{coil})\, r\, dr \; . \tag{38}$$

At high pressure, when $\omega \ll \nu$, the plasma conductivity is mainly active and the whole problem of Eqs. (26) and (35) corresponds to the ordinary skin effect in nonuniform, nonlinear media with conductivity Σ_1, which is determined by the amplitude of the external current in the coil. At lower pressures, the reactive (inductive) nonlinear plasma conductivity Σ_2 dominates in Eq. (26), which corresponds to the account of electron inertia. As was stated before, our approximation, Eq. (26), is applicable even in this case, if only the skin layer is not too thin [see Eq. (2)]. In any case, the effective skin layer thickness δ can be estimated as

$$\delta \sim (\mu_0 \omega \mid \Sigma \mid)^{-1/2} \; . \tag{39}$$

In the semi-infinite plasma the conditions $\delta < \lambda\nu/\omega, \lambda$ are sufficient for the existence of the anomalous skin effect [54]. In this case the electron energy gains and losses during the collisionless passage of the skin layer can be treated as statistically independent and the electromagnetic energy is transferred from the field to the electrons. The active part of the plasma impedance Σ_1 arises even in the absence of collisions. However, our case of a spatially bounded plasma is more complicated. Situations are possible when the energy gains and losses during the subsequent electron passages through the skin layer are correlated and the active part of the plasma impedance is considerably diminished with respect to the classical value [54].

D. Numerical scheme

From the above-mentioned system of equations, a self-consistent set of solutions consisting of the EDF of total energy $F_0^{(0)}(\varepsilon)$, the space-charge potential $\Phi(r)$, and the profile of the rf field $E(r)$ can be found. To cope with the mutual interdependencies, an iterative method has been developed, which is sketched in the flow diagram in Fig. 3. The method takes advantage of the fact that some
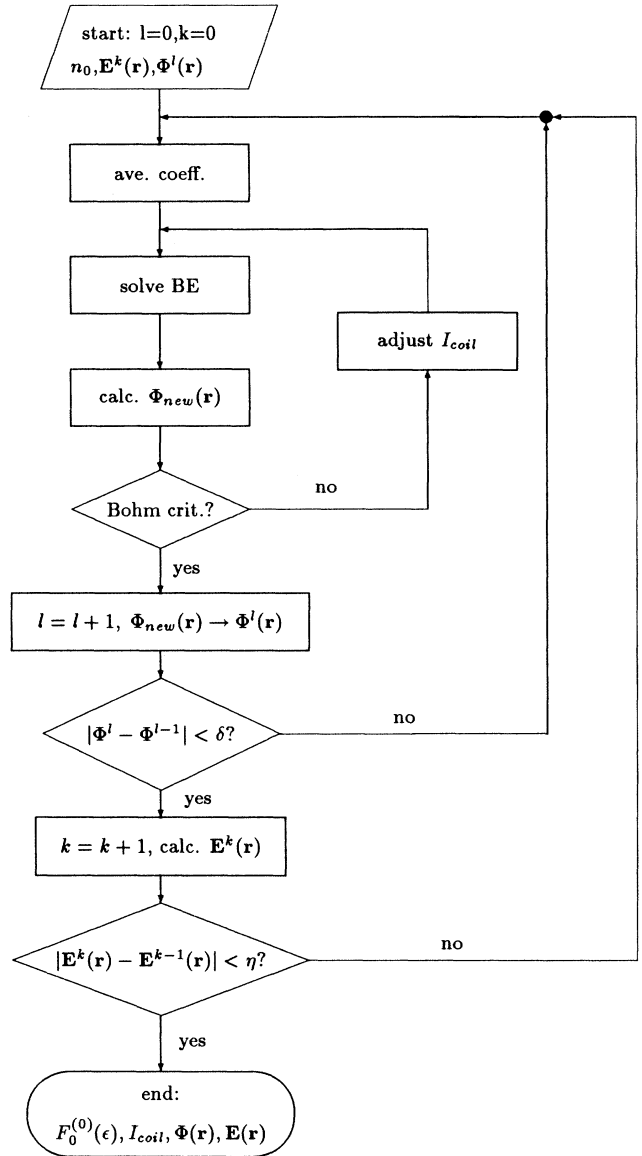

FIG. 3. Flow diagram of the two-dimensional model of a RFI discharge.

quantities — namely the spatially averaged coefficients in the kinetic equation (15) — depend on others only via integral formulations. The exact shape of the spatial profiles is therefore not of great importance. Hence, the EDF should be not too sensitive to the exact profiles of the rf field and the space-charge potential. It is thus reasonable to perform the calculation of the EDF in an inner loop and the exact determination of the field and the potential profiles in outer loops. Changes in these profiles affect the EDF only slightly, which guarantees a fast and stable convergence of the iterative scheme.

The EDF at a given value of the central plasma density n_0 is determined via the solution of Eq. (15) (denoted BE for Boltzmann equation) in the interior loop. The averaged coefficients are calculated with some start-

ing profiles for the rf electric field and the potential, e.g., a flat rf field and a parabolic potential. After the solution of Eq. (15) an ionization profile (33) can be obtained from the EDF and the old potential profile. Equations (27) and (28) can then be integrated to find a new potential and plasma density distribution. This procedure is repeated, while varying the coil current I_{coil}, until the Bohm criterion is fulfilled at the position of the wall. (The sheath is assumed to be infinitely thin, which causes a negligible uncertainty for I_{coil}.) The resulting potential profile is used to reevaluate the averaged coefficients. This whole loop of solving the kinetic equation, adjusting I_{coil}, and calculating a new potential profile is repeated, until convergence in the space-charge potential is achieved. Usually about four to six iterations are sufficient to obtain a relative accuracy of the potential of better than 0.01%. By using this procedure, a self-consistent set of an EDF, I_{coil}, and a potential profile is obtained, with the values of R, L, the pressure p, and n_0 being given. The profiles of $\Phi(\mathbf{r})$, $E_0(\mathbf{r})$, $n(\mathbf{r})$, and the value of n_0 can afterwards be found for the given external parameters $(R, L, p, \text{and } I_{coil})$. In the outer loop the rf electric field distribution is determined with the radial density profiles from Eq. (27) by integrating Eq. (34). The loop is repeated until the rf field distribution is also self-consistently determined. Usually about four iterations are needed to achieve a relative accuracy of better than 0.1% for the rf field profile. The wall potential Φ_w and the escape term Eqs. (33) and (34) were not accounted for in the presented simplest calculations.

The numerical scheme presented above turned out to be quite efficient. For one set of parameters the complete problem is solved within typically 40 min on a 486DX PC (66 MHz). The most serious computational difficulties were connected not with the solution of the electron Boltzmann equation, but with the ion transport equation combined with the quasineutrality condition, due to the use of the realistic field-dependent ion mobility. For comparison, it should be mentioned that the computation times are probably some orders of magnitude smaller than those of other Monte Carlo based [11,12] or time-dependent fluid models [42]. From a physical point of view, the computation time might not be a decisive argument for one model or the other. However, to obtain a general understanding of the discharge and to design a particular device it is necessary to perform scans over wide parameter ranges. Examples where two parameters have to be varied are, for instance, the simple calculations of current-voltage characteristics of the discharge for various gas pressures. For these purposes the computation time is of principal importance.

IV. EXPERIMENTAL AND THEORETICAL RESULTS AND DISCUSSION

The central point of the two-dimensional (2D) model presented consists of the description of the electron kinetics. Thus it is of highest priority for the experiment to prove or disprove its validity. In Fig. 4 the EDFs obtained from the present model and measurements performed in
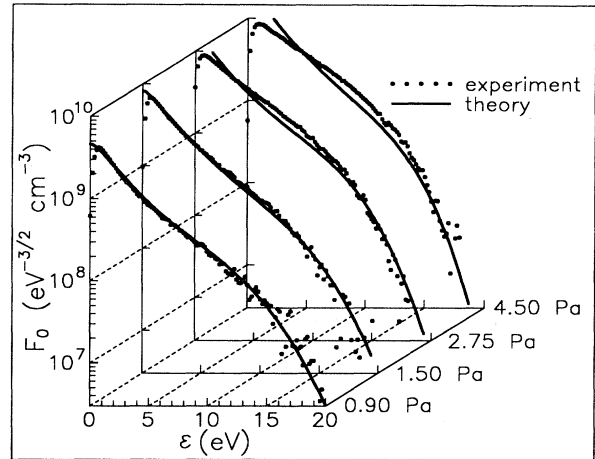

FIG. 4. Comparison between measured EDFs and results of the 2D model in the center of the discharge.

the center of the discharge are compared. It is obvious that a convincing quantitative agreement is obtained. In particular, for the lower pressures the coincidence of experiment and theory is excellent. For higher pressures some deviations occur, in particular at low kinetic energies where the experimental EDF does not exhibit such a pronounced peak as has been predicted by the theory. However, it is well known that the main problems of the experimental measurement of the EDF appear close to zero kinetic energy. It should be mentioned that the theoretical EDFs are normalized to the same electron density as the experimental results. Indeed, the central electron density is self-consistently calculated as a function of the absorbed power (or more precisely vice versa, see Sec. III C), but it is too optimistic to expect that the theoretical and experimental electron density would coincide within a few percent. This point is discussed in more detail below. In order to judge the quality of the electron kinetic model it is thus appropriate to normalize experimental and theoretical results to the same density.

The qualitative behavior of the observed EDFs is quite reasonable. It is clearly seen that the exponential decrease begins at $\epsilon \approx u_1$. The growth of EDF at low values of ϵ is connected with the decrease of the spatially averaged energy diffusion coefficient (10) due to the Ramsauer effect (especially at low pressures) and to the decrease of the accessible volume V_{ac}, Eq. (12). A similar behavior has been observed also in [50].

A crude estimate for the EDF form can be obtained if we neglect the variation of V_{ac}, assume approximately $\omega \ll \nu$ and $\nu \sim v^3$, and replace the right-hand side of Eq. (15) by a zero boundary condition at $\epsilon \approx u_1$. The corresponding mean value of the kinetic energy in the center of ≈ 5 eV is very close to the observed values (from 4.5 to 5.5 eV).

In Fig. 5, experimental and theoretical results for the axial and the radial variation of the EDF are given. For reasons of clearness the axial variation of the EDFs is plotted only on one side of the midplane. The behavior of the EDFs on the other side of the midplane is identical
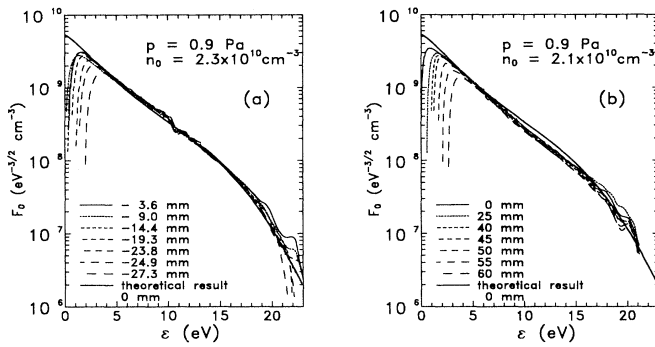
FIG. 5. Axial (a) and radial (b) variation of the EDF in the RFI discharge. The thick lines represent the theoretical results. The coil current is $I_{coil} = 7.3A$.

and contains no additional information. From Fig. 5 it is obvious that the EDFs in the radial as well as in the axial direction can be considered dependent only on the total energy, at least within experimental error. Furthermore, the coincidence of the measured EDFs with the theoretical results is quite convincing. Thus the results presented in Fig. 5 confirm the applicability of the non-

local approach to the description of the electron kinetics, which is one central simplification of the present model. It should be mentioned that the differences between electron densities obtained for the same experimental parameters probably stem from the fact that different probes have been used for the radial and axial scans. Changing the probes, however, is always connected to changing the characteristics of the probe system itself and of the whole experiment.

Measured and calculated profiles of the space-charge potential and of the electron density are presented in Figs. 6 and 7. The electron densities have been obtained by integration of the measured EDF; the space-charge potential profile is obtained from the shift of the zero crossing of the measured second derivatives. For both pressures good agreement of the experimental and theoretical results is obtained for both the radial and the axial variations. As expected, the density decreases faster towards the walls for the higher pressure of 3 Pa. Also, the variation of the potential is more pronounced. The experimental results, in particular for 3 Pa, confirm that the potential and electron density vary more strongly in radial rather than in the axial direction due to the aspect ratio of our discharge.

In Fig. 8 the calculated profiles of the ambipolar space charge potential and the related electron density distribution are given. It should be remembered that the elec-
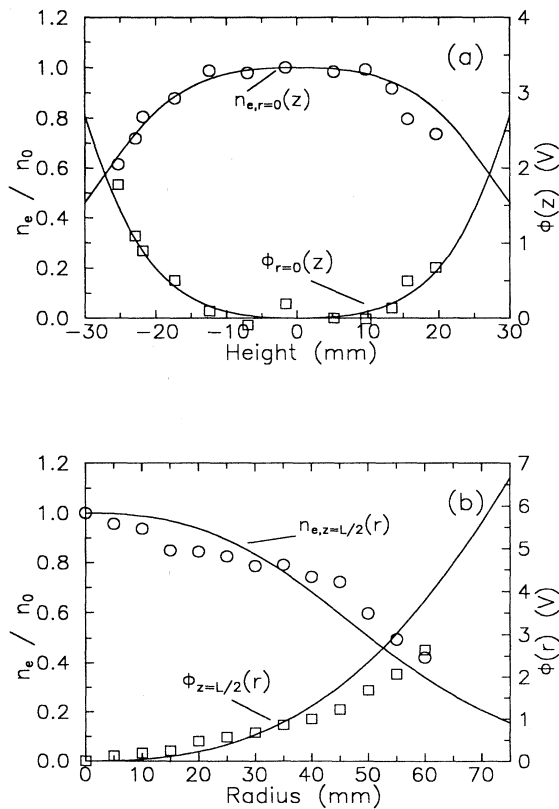

FIG. 6. Profiles of the space-charge potential and the electron density for $p = 0.9$ Pa: (a) axial and (b) radial. The solid lines represent the results of the 2D model. The circles represent the experimental electron density profile, the squares the measured potential profile.
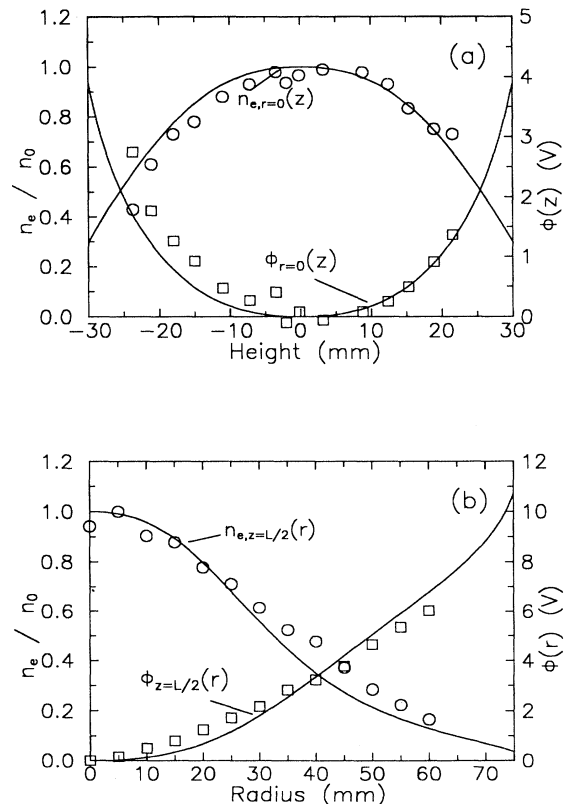

FIG. 7. Profiles of the space-charge potential and the electron density for $p = 3.0$ Pa. The representation and notation are the same as in Fig. 6.
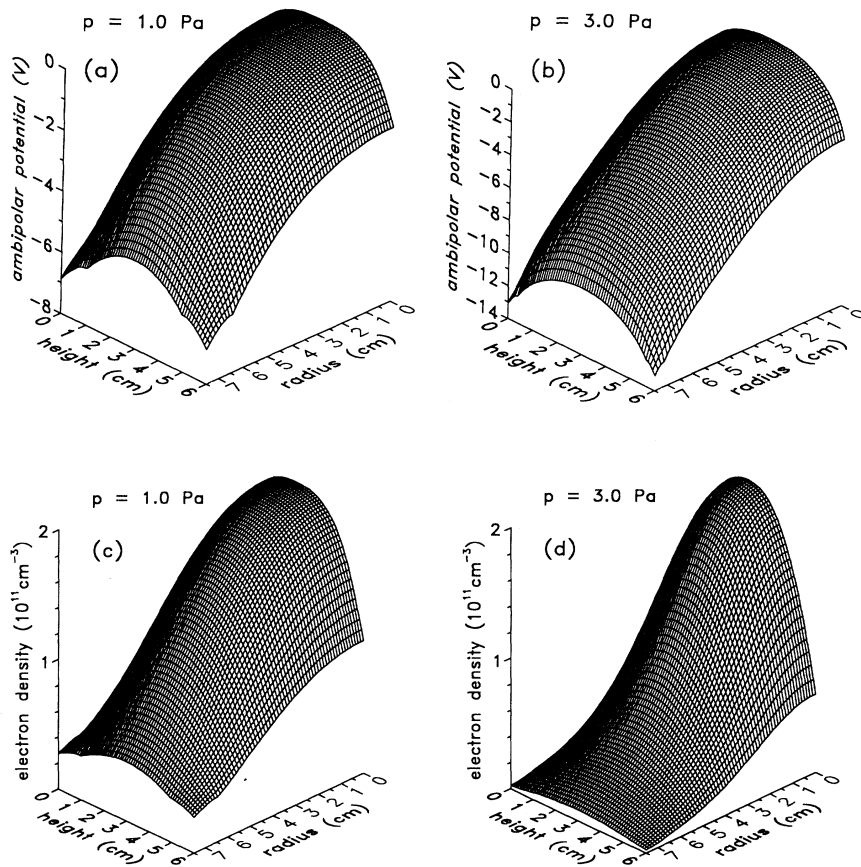
FIG. 8. Profiles of the ambipolar space-charge potential [(a), (b)] and the related electron density [(c), (d)] for $p = 1$ Pa and 3 Pa.

tron density and the space-charge potential profile are plotted up to the plasma-sheath boundary only. (The small kinks close to the edges of the profiles at 1 Pa are numerical "edge effects.") The differences in the radial and axial density distribution are clearly seen. From one-dimensional models of the ambipolar diffusion (e.g., for a positive column) it is well known that the density at the plasma sheath boundary scales roughly with the ratio of the ion mean free path to the diffusion length λ_i/Λ (e.g., [68]). If this scaling law is applied to the considered discharge ($L/2 = 3$ cm, $R = 7.5$ cm), the differences between the electron density at the sheath boundary on the axis (r

$= 0$ cm, $z = 0$ or 6 cm) and at the side wall in the midplane of the discharge ($r = R$, $z = 3$ cm) should be of the order of a factor 2. This is approximately fulfilled for the lower pressure of 1 Pa. However, for the higher pressure of 3 Pa the density at the side walls is much lower than expected from this simple scaling law. The reason may be seen in the fact that the ionization at 3 Pa is strongly concentrated in the center of the discharge, where the electron density is maximal (see Fig. 9). Qualitatively, the situation can be understood if a point source of ionization in the center of the discharge is considered. For the present aspect ratio, the diffusion in the axial direction can be
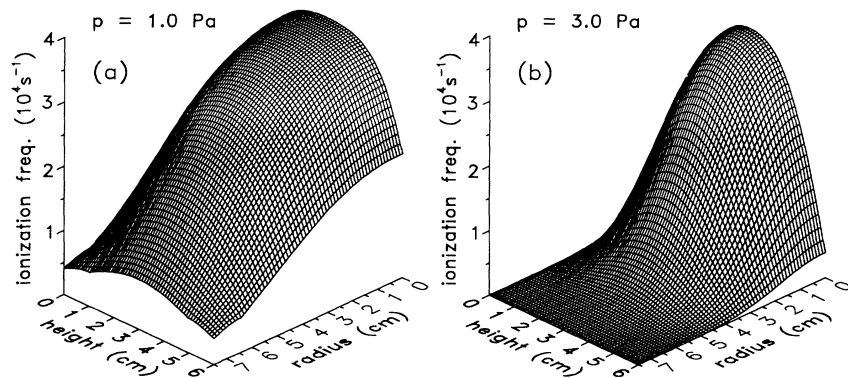

FIG. 9. Spatial distribution of the ionization frequency: (a) 1 Pa and (b) 3 Pa.

considered as an almost one-dimensional problem. For the radial diffusion, however, the two-dimensional effects cannot be neglected. Ions which are generated in the center are first of all diluted due to the geometrical effects of the diffusion in cylindrical geometry. However, a second diluting effect is the permanent drain of ions in the axial direction during their radial diffusion. This effect is much less pronounced for lower pressures, where the ionization is more homogeneously distributed across the whole discharge. The potential profile adjusts itself to guarantee quasineutrality, i.e., to screen the electrons to a sufficient degree. Thus the strong dilution of ions at high pressures during their radial diffusion requires a strong drop of the potential in the radial direction. So, for instance, at 3 Pa the sheath boundary potential on the axis is -3.8 V, while at the side wall in the midplane it is -10.0 V. Again, this effect is less pronounced for lower pressures due to the more homogeneous ionization profile. A similar radial decrease of the plasma density, which was close to exponential, was observed for large values of the R/L ratio in [69].

As was discussed in the Introduction and is seen from the results of our model (Figs. 6–9), independent of the energy input profile, the profiles of the plasma density $n(r, z)$, of the stationary potential $\Phi(\mathbf{r})$, and of the plasma source term $n\nu_i(\mathbf{r})$ in Eq. (28) are maximal in the discharge center in the nonlocal approximation. This conclusion is connected with the fact that the coefficients in Eqs. (27), (28), and (33), which determine the potential profile, depend only on $\Phi(r, z)$ but not on (r, z) explicitly. It results in the symmetry of the solution. The experimental data are in reasonable agreement with this statement. The slight asymmetry in the axial density and potential profile in Fig. 7 can be produced by some subtle effects, such as remnants of the locality, the asymmetry in the high-energy part of the EDF, which is generated by different boundary conditions on the metal and dielectric surfaces, and a partial restoration of the fluid approach due to the electron-electron collisions. (The most striking peculiarity of the observed asymmetry consists of the fact that it is practically independent of the power input.)

In [31] the existence of two maxima in the light emission was reported. The first of them was situated at the chamber axis at $z \approx L/2$, and the second was close to the maximum of the rf field. The intensity of the latter increased with pressure. This phenomenon can be also explained as the start of the transition from the nonlocal to the local regime.

In the nonlocal case the considerable distance between the chamber center and the position of the maximal energy input manifests itself not in a shift of the plasma density profile but in the formation of a cold plasma in the center of the discharge. This phenomenon was discussed in [70,25,71,31]. It can be explained as follows. In the scale of the full energy the electrons with small ϵ are trapped by the ambipolar field in the vicinity of the discharge center. If the rf field is maximal at the periphery, they cannot reach this region and their spatially averaged energy diffusion coefficient D_ϵ [Eq. (10)], which is proportional to the square of the rf field, is small. It results in a steep decrease of $F_0^{(0)}(\epsilon)$, i.e., a low "effective

temperature," in the low-energy part of the EDF.

It is necessary to stress here that all these phenomena cannot be described properly in the framework of the fluid approach, when all the electrons are characterized by the average values of the directed velocity and of the mean energy [71]. In the nonlocal case, when the EDF depends mainly on ϵ, the source term in Eq. (15) is maximal in the chamber center. After inelastic collisions, the slow electrons gain energy in the rf field due to the energy diffusion process. The growth of the accessible volume V_{ac} [Eq. (12)] with increasing energy corresponds to an outward-directed electron flux at $\epsilon < u_1$. At higher energies, however, the intensive process of inelastic collisions is switched on. It is maximal in the chamber center and an inward-directed flux of the fast electrons with $\epsilon > u_1$ arises.

The two-dimensional structure of the rf electric field is depicted in Fig. 10 for two different central plasma densities $n_0 = 1 \times 10^{11}$ cm^{-3} (top) and $n_0 = 1 \times 10^{12}$ cm^{-3} (bottom). (Note that not the field lines but the lines of
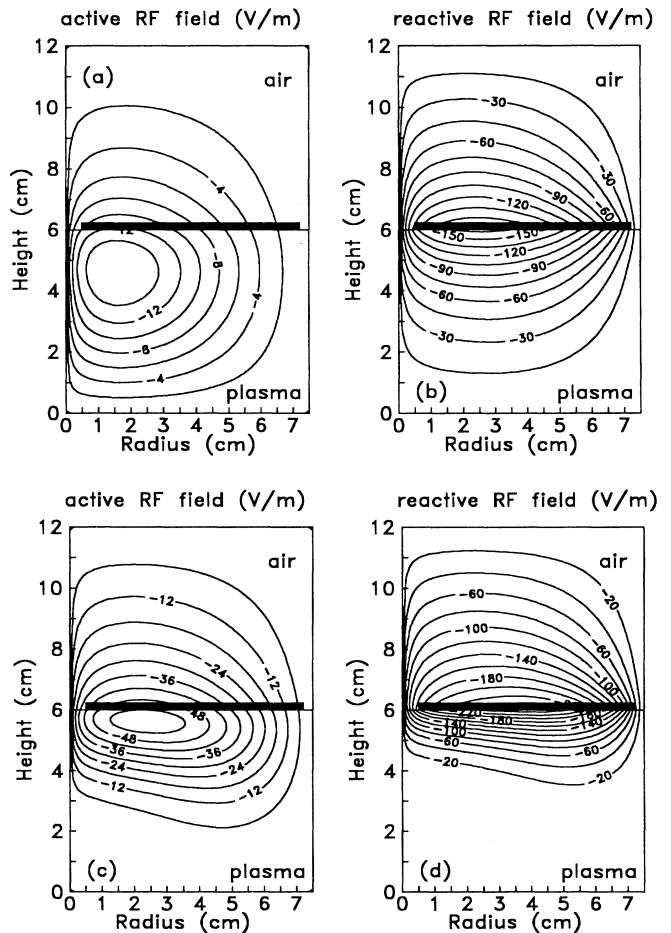

FIG. 10. Profiles of the rf electric field: active part [(a), (c)], reactive part [(b), (d)]. The central plasma density for the upper figures is $n_0 = 1 \times 10^{11}$ cm^{-3} for the lower figures $n_0 = 1 \times 10^{12}$ cm^{-3}. The thick lines represent the position of the flat coil ($R_1 = 0.5$ cm and $R_2 = 7.2$ cm).

constant field strength are plotted.) The coil is assumed
to be separated from the plasma by an infinitely thin
glass plate. The figures on the left side represent the real
(active) part of the electric field, which is shifted by $-\pi/2$
with respect to I_{coil}, and the figures on the right side rep-
resent the imaginary (reactive or inductive) part of the
electric field, which is the opposite of I_{coil}. While the
reactive field is responsible for the apparent power, the
active field is connected with the absorbed power. The
latter results from the collisions of plasma electrons with
heavy particles. Considering first the reactive part of the
field at $n_0 = 1 \times 10^{11}$ cm^{-3}, the approximate symmetry
of the field distribution in the plasma and the air is ob-
vious. In this case the electron density is still too small
to cause a considerable skin effect. The maximum of the
reactive field is, of course, found at the induction coil,
since the rf current is the source of this field component.
For the higher plasma density $(n_0 = 1 \times 10^{12}$ cm$^{-3})$ a
strong skin effect occurs. It should be remembered that
the discharge center and thus the maximum of the elec-
tron density is located at $r = 0$ cm and $z = 3$ cm. The
density profile finds its correlation in the asymmetry of
the electric field. It is more strongly "repelled" from the
plasma close to the center than at the discharge edge,
where the electron density is small. While the reactive
part of the field is maximal close to the coil, the active
part has its maximum inside the plasma. This behavior is
quite reasonable, since the active field is associated with
the resistive part of the plasma current, i.e., that part
which is generated by collisions of the electrons with the
heavy particles. This component of the current is $-\pi/2$
out of phase with the rf current in the induction coil and
thus in phase with the reactive component of the electric
field. It is not surprising that the maximum of the active
field is found somewhere between the maximum of the
electron density $(r = 0$ cm, $z = 3$ cm$)$ and the maximum
of the reactive field component (the induction coil). It
can be seen in Fig. 10 that with increasing electron den-
sity the maximum of the active field shifts towards the
outer plasma regions closer to the coil since the reactive
field is "pushed" out of the plasma by the skin effect. In
experiments in Ref. [72] the considerable skin effect of the
magnetic field B_r, which increased with the power input,
was investigated. It is in qualitative agreement with our
calculations.

One particular interesting aspect of the discharge con-
struction is the discharge impedance and the relation be-
tween absorbed power and achieved electron density. The
first point is studied in Fig. 11. The real and imaginary
parts of the discharge impedance are plotted against the
total rf power. Both quantities have been determined
by measuring the rf current (via a current transformer)
and the rf voltage (via a capacitive voltage divider) and
the phase angle between them, using a network analyzer.
It should be remembered that the total rf power is not
equal to the absorbed power. Since the power factor
$\cos\phi$ is very small, namely ≤ 0.02, only about 2% of
the depicted total power is really absorbed. Thus the
main part of the power is apparent power. The high
rf currents, which are connected to the high apparent
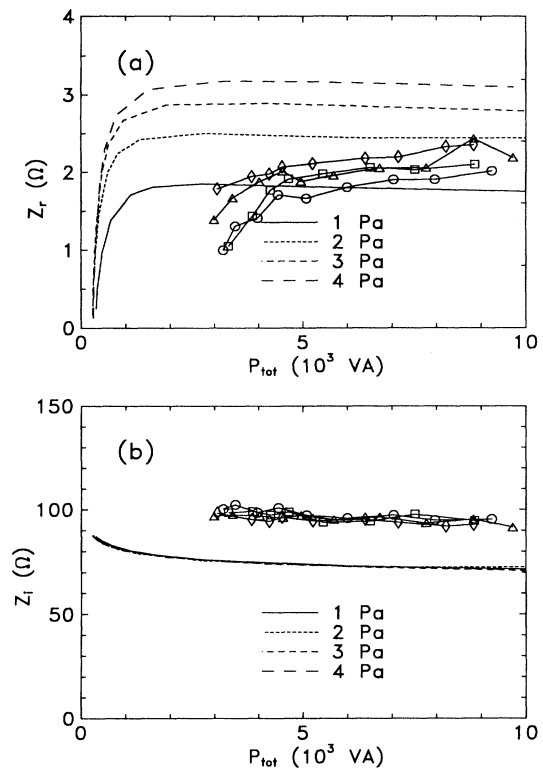power, lead to a considerable thermal load of the electric

FIG. 11. Real (a) and imaginary (b) parts of the discharge
impedance as a function of the total rf power $P_{tot} = UI/2$.
The symbols denote the experimental results: 1 Pa (o), 2 Pa
($\square$), 3 Pa ($\triangle$), and 4 Pa ($\Diamond$).

circuit, in particular, of the matching network. As can
be seen in Fig. 11 the agreement between experimental
values of the impedance and the theoretical predictions
is reasonable. In particular, one has to remember that
some crude assumptions have been made concerning the
coil geometry (plane coil) and the boundary conditions
(closed metallic screen) which do not exactly correspond
to the experimental situation. Thus an accuracy of about
30% for the reactive part of the impedance is a satis-
factory result. One should bear in mind that the de-
termination of the inductance of a planar coil with the
present two-dimensional boundary conditions is a non-
trivial problem. The experimental values for the resistive
part of the impedance and their theoretical predictions
agree within a factor 2. The experimental results confirm
the decrease of Σ_1 with increasing neutral density. As
mentioned before, one reason for the deviations between
experiment and theory may be seen in the simplifying as-
sumptions used in the model. However, the experimental
errors of the active part are also surely larger than for the
reactive part, since the measured phase angles between
current and voltage have been quite close to 90° (about
87°–89°). Since the experimental accuracy of the phase
angle measurement is about 0.5°, the relative error for
the resistive part of the impedance is much higher than
for the reactive part.

Finally, the most delicate aspect of self-consistent

plasma models should be discussed. It is well known that even with very sophisticated self-consistent plasma models the electron density observed in experiments is usually not better predicted than up to a factor 2 or 3. Recently it has been pointed out by Surendra [73] that self-consistent models developed for one and the same physical situation of a capacitively coupled rf discharge (in particular, using the same cross section data) may yield self-consistent densities which differ by more than a factor 4. Thus no more should be expected from the present 2D model. The experimentally and theoretically determined electron densities as a function of the absorbed power are depicted in Fig. 12. Unfortunately, the experimentally obtained electron densities are about a factor of 4 lower than the theoretically predicted values. Indeed, the measurements confirm at least qualitatively some trends predicted by the theory. Thus the linear dependence of the electron density on the absorbed power is consistent with the measurements. Also, the increase of the electron density with the neutral gas pressure at constant absorbed power is evidenced by the measurements. The reasons for the quantitative deviations are numerous and can be found on both the experimental and the theoretical sides. First of all, the experimental density measurement is never free of some errors. In the discussion above it has been shown that the experimental resolution of the low-energy part of the EDF deteriorates with increasing pressure and input power. To correct these deviations in the low-energy range some extrapolation of the EDF towards zero kinetic energy is necessary. Furthermore, the temperature of the neutral gas is another factor of uncertainty. For the comparison between measurements and numerical results where the neutral density rather than the pressure is involved, a gas temperature of 300 K has been assumed. For the higher electron densities of the order of $n_e \approx 10^{11}$ cm^{-3}, this assumption becomes questionable. When the pressure is measured, a higher gas temperature corresponds to a lower neutral density. In this case the experimental points would have to be compared to theoretical curves of a lower neutral density, i.e., lower pressure in Fig. 12. This would give a correction in the right direction. An-

other uncertain point is the assumption that the entire amount of absorbed power measured is really absorbed by the plasma. The electrical characteristics have been measured as close as possible to the coil. Nevertheless, the coil structure also absorbs some amount of the delivered power. At the moment no detailed information about the fraction of power absorbed by the coil structure is available but the thermal loading of the coil is substantial so that cooling by compressed air is necessary.

Detailed measurements of the discharge impedance were performed by Godyak et al. [55]. Their results are more or less in qualitative agreement with our results. At low input power the skin effect is absent and the rf field is simply proportional to the value of I_{coil}. Since the plasma contribution to the total impedance is also small, it means, that the self-sustained discharge in the absence of the skin effect is possible only at the fixed values of the coil voltage and current. This fact can be noticed in the results of Ref. [55]. Their measured impedance was close to 70 Ω. It is in good agreement with the measured value of the impedance of the unloaded coil of 85 Ω. From their measurements at the low power levels the authors estimated the ratio ω/ν. The power input per electron is, according to Eqs. (26) and (35), proportional to $I_{coil}^2 \nu/(\omega^2 + \nu^2)$. It has to be equal to ϵ_0/τ, where ϵ_0 is the ionization price and τ the mean ambipolar electron lifetime. If we assume, in a crude approximation, $\omega/\nu = 0.017/p$ (for $\omega/2\pi = 13.56$ MHz and p in Torr) and $\epsilon_0 =$ const, we obtain the following values of the ratio $I_{coil}(p)/I_{coil}(p = \infty)$: 1.05, 2.0, and 5.5 at pressures of 0.1, 0.01, and 0.003 Torr. The corresponding experimental values of [55] are 1.2, 2.1, and 2.8. The considerable distinction in the last numbers (2.8 instead of 5.5) can be attributed to the existence of some additional collisionless stochastizing mechanism. However, the decrease of ϵ_0 at low pressures can also lead to the observed decrease of the above-mentioned ratio. Keeping in mind also that, as discussed above, the collisionless stochastization mechanism in the spatially bounded plasma cannot be reduced completely to the anomalous skin effect, more detailed investigations in this direction are very desirable.

V. CONCLUSIONS

In this paper we have presented a fast self-consistent kinetic model for the description of low-pressure inductively coupled rf discharges. A high efficiency of our model was achieved by using consistently the given physical information. By accounting for the nonlocality and the time independence of the EDF from the very beginning, it was possible to reduce the complete multidimensional problem of the electron kinetics to the simple solution of a one-dimensional ordinary differential equation. By taking advantage of the strict division of the discharge volume into the quasineutral plasma and space-charge sheaths we were able to avoid the complicated and tedious straightforward integration of the Poisson equation. The obtained system of equations was comparatively simple and could even be solved by relatively slow
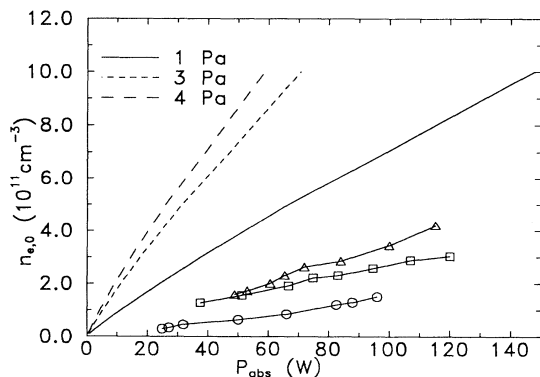
FIG. 12. Experimental and theoretical central electron densities. The symbols denote the experimental results: 1 Pa (○), 3 Pa (□), and 4 Pa (△).

computers such as a usual PC (486DX, 66 MHz) within computation times of some 10 min.

The quantitative accuracy of the presented model has been demonstrated by a number of comparisons to experimental data. In particular, the validity of the nonlocal approach to the electron kinetics has been proven by the good agreement between calculated and spatially resolved measured EDFs. Also, for the electron density and space-charge potential profile distribution a convincing agreement has been demonstrated.

The fact that the presented model is, by some orders of magnitude, faster than other straightforward models proves the value of the chosen strategy: to employ all available physical information from the very beginning. Such a fast and efficient model as the one presented above offers the possibility of a thorough analysis and understanding of most of the physical principles by variation of various parameters. Furthermore, keeping in mind the present short computation times, there is still a lot of room left for refinements as an account of deviations from the nonlocality in a first order correction or the implementation of plasma chemistry.

ACKNOWLEDGMENTS

[1] B. N. Chapman, *Glow Discharge Processes* (Wiley, New York, 1980).

[2] D. B. Graves, IEEE Trans. Plasma Sci. **22**, 31 (1994).

[3] J. Hopwood, Plasma Sources Sci. Technol. **1**, 109 (1992).

[4] O. A. Popov, J. Vac. Sci. Technol. A **7**, 894 (1989).

[5] T. J. Sommerer, W. N. G. Hitchon, and J. E. Lawler, Phys. Rev. Lett. **63**, 2361 (1989).

[6] T. J. Sommerer, W. N. G. Hitchon, and J. E. Lawler, Phys. Rev. A **39**, 6356 (1989).

[7] M. Surendra and D. B. Graves, IEEE Trans. Plasma Sci. **19**, 144 (1991).

[8] M. Surendra and D. B. Graves, Appl. Phys. Lett. **59**, 2091 (1991).

[9] W. N. G. Hitchon, G. J. Parker, and J. E. Lawler, IEEE Trans. Plasma Sci. **21**, 228 (1993).

[10] G. J. Parker, W. N. G. Hitchon, and J. E. Lawler, Phys. Fluids B **5**, 646 (1993).

[11] P. L. G. Ventzek, T. J. Sommerer, R. J. Hoekstra, and M. J. Kushner, Appl. Phys. Lett. **63**, 605 (1993).

[12] P. L. G. Ventzek, R. J. Hoekstra, and M. J. Kushner, J. Vac. Sci. Technol. B **12**, 461 (1994).

[13] V. Vahedi, G. DiPeso, C. K. Birdsall, M. A. Liebermann, and T. D. Rognlien, Plasma Sources Sci. Technol. **2**, 261 (1993).

[14] V. Vahedi, C. K. Birdsall, M. A. Liebermann, G. DiPeso, and T. D. Rognlien, Plasma Sources Sci. Technol. **2**, 273 (1993).

[15] V. A. Feoktistov, A. M. Popov, O. B. Popovicheva, A. T. Rakhimov, T. V. Rakhimova, and E. A. Volkova, IEEE Trans. Plasma Sci. **19**, 163 (1991).

[16] G. Gousset, C. M. Ferreira, M. Pinheiro, P. A. Sá, M. Touzeau, M. Vialle, and J. Loureiro, J. Phys. D **24**, 290 (1991).

[17] P. Belenguer and J. P. Boeuf, Phys. Rev. A **41**, 4447 (1990).

[18] M. Capitelli, M. Dilonardo, R. Winkler, and J. Wilhelm, Contrib. Plasma Phys. **26**, 443 (1986).

[19] M. Capitelli, C. Gorse, R. Winkler, and J. Wilhelm, J. Appl. Phys. **62**, 4398 (1987).

[20] I. B. Bernstein and T. Holstein, Phys. Rev. **94**, 1475 (1954).

[21] L. D. Tsendin, Zh. Eksp. Teor. Fiz. **66**, 1638 (1974) [Sov. Phys. JETP **39**, 805 (1974)].

[22] K. Wiesemann, Ann. Phys. (Leipzig) **23**, 275 (1969).

[23] V. A. Godyak and R. B. Piejak, Appl. Phys. Lett. **63**, 3137 (1993).

[24] U. Kortshagen, Phys. Rev. E **49**, 4369 (1994).

[25] U. Kortshagen, I. Pukropski, and M. Zethoff, J. Appl. Phys. **76**, 2048 (1994).

[26] L. D. Tsendin and Y. B. Golubovskii, Zh. Tekh. Fiz. **47**, 1839 (1977) [Sov. Phys. Tech. Phys. **22**, 1066 (1977)].

[27] J. Behnke and Y. B. Golubovskij, Zh. Tekh. Fiz. **64**, 166 (1994) [Sov. Phys. Tech. Phys. **39**, 38 (1994)].

[28] L. D. Tsendin, Zh. Tekh. Fiz. **56**, 278 (1986) [Sov. Phys. Tech. Phys. **31**, 169 (1986)].

[29] Y. B. Golubovskij, S. H. Al-Hhavat, and L. D. Tsendin, Zh. Tekh. Fiz. **57**, 1285 (1987) [Sov. Phys. Tech. Phys. **32**, 760 (1987)].

[30] V. I. Kolobov and L. D. Tsendin, Phys. Rev. A **46**, 7837 (1992).

[31] V. I. Kolobov, D. F. Beale, L. J. Mahoney, and A. E. Wendt, Appl. Phys. Lett. **65**, 537 (1994).

[32] U. Kortshagen and L. D. Tsendin, Appl. Phys. Lett. **65**, 1355 (1994).

[33] S. V. Berezhnoi, I. D. Kaganovich, E. L. Levin, and L. D. Tsendin, in *Proceeding of the 1994 International Conference on Plasma Physics*, edited by P. H. Sakanake, E. D. Besco, and M. V. Alves (unpublished).

[34] A. S. Smirnov and L. D. Tsendin, Zh. Tekh. Fiz. **60**, 56 (1990) [Sov. Phys. Tech. Phys. **35**, 786 (1990)].

[35] A. S. Smirnov and L. D. Tsendin, Zh. Tekh. Fiz. **61**, 64 (1991) [Sov. Phys. Tech. Phys. **36**, 284 (1991)].

[36] A. S. Smirnov and L. D. Tsendin, IEEE Trans. Plasma Sci. **19**, 130 (1991).

[37] I. D. Kaganovich and L. D. Tsendin, IEEE Trans. Plasma Sci. **20**, 66 (1992).

[38] J. H. Keller, J. C. Forster, and M. S. Barnes, J. Vac. Sci. Technol. A **11**, 2487 (1993).

[39] J. B. Carter, J. P. Holland, E. Peltzer, B. Richardson, H. T. Nguyen, Y. Melaku, D. Gates, and M. Ben-Dor, J. Vac. Sci. Technol. A **11**, 1301 (1993).

[40] C. T. Gabriel and Y. Melaku, J. Vac. Sci. Technol. B **12**,

454 (1994).

[41] M. S. Barnes, J. C. Forster, and J. H. Keller, Appl. Phys. Lett. **62**, 2622 (1993).

[42] R. A. Stewart, P. Vitello, and D. B. Graves, J. Vac. Sci. Technol. B **12**, 478 (1994).

[43] A. P. Zhilinsky, I. F. Liventseva, and L. D. Tsendin, Zh. Tekh. Fiz. **47**, 304 (1977) [Sov. Phys. Tech. Phys. **22**, 177 (1977)].

[44] G. Oelerich-Hill, I. Pukropski, and M. Kujawka, J. Phys. D **24**, 593 (1991).

[45] K. F. Schoenberg, Rev. Sci. Instrum. **49**, 1377 (1978).

[46] V. A. Godyak, R. B. Piejak, and B. M. Alexandrovich, Phys. Rev. Lett. **68**, 40 (1992).

[47] R. R. J. Gagné and A. Cantin, J. Appl. Phys. **43**, 2639 (1972).

[48] A. P. Paranjpe, J. P. McVittie, and S. A. Self, J. Appl. Phys. **67**, 6718 (1990).

[49] G. Dilecce, M. Capitelli, and S. D. Benedictis, J. Appl. Phys. **69**, 121 (1991).

[50] V. A. Godyak, R. B. Piejak, and B. M. Alexandrovich (private communication).

[51] Y. M. Aliev, V. Y. Bychenkov, A. V. Maximov, and H. Schlüter, Plasma Sources Sci. Technol. **1**, 126 (1992).

[52] Y. M. Aliev, A. V. Maximov, and H. Schlüter, Phys. Scr. **48**, 464 (1993).

[53] M. M. Turner, Phys. Rev. Lett. **71**, 1844 (1993).

[54] E. M. Lifshitz and Pitajewski, *Physikalische Kinetik* (Akademie-Verlag, Berlin, 1983).

[55] V. A. Godyak, R. B. Piejak, and B. M. Alexandrovich, Plasma Sources Sci. Technol. **3**, 169 (1994).

[56] L. D. Tsendin, Zh. Eksp. Teor. Fiz. **47**, 1598 (1977) [Sov. Phys. Tech. Phys. **22**, 925 (1977)].

[57] V. Kolobov and W. N. G. Hitchon (private communication).

[58] I. P. Shkarofsky, T. W. Johnston, and M. P. Bachynski, *The Particle Kinetics of Plasmas* (Addison-Wesley, Reading, MA, 1966).

[59] L. D. Tsendin, Zh. Eksp. Teor. Fiz. **48**, 1569 (1978) [Sov. Phys. Tech. Phys. **23**, 890 (1978)].

[60] E. W. McDaniel, *Collision Phenomena in Ionized Gases* (Wiley & Sons, New York, 1964).

[61] V. Martisovits, J. Phys. B **3**, 850 (1970).

[62] P. A. Sá, J. Loureiro, and C. M. Ferreira, J. Phys. D **25**, 960 (1992).

[63] A. Böhle and U. Kortshagen, Plasma Sources Sci. Technol. **3**, 80 (1994).

[64] K.-U. Riemann, J. Phys. D **24**, 493 (1991).

[65] U. Kortshagen, Plasma Sources Sci. Technol. **4**, 172 (1995).

[66] J. Krenz, University of Hannover, Report No. 13N54069, 1987 (unpublished).

[67] J. D. Jackson, *Classical Electrodynamics* (Wiley, New York, 1975).

[68] V. E. Golant, A. P. Zhilinsky, and I. E. Sakharov, *Fundamentals of Plasma Physics* (John Wiley & Sons, New York, 1980).

[69] P. N. Wainman, M. A. Lieberman, A. J. Lichtenberg, R. A. Stewart, and C. Lee (private communication).

[70] U. Kortshagen, J. Phys. D **26**, 1230 (1993).

[71] L. D. Tsendin, Plasma Sources Sci. Technol. **4**, 200 (1995).

[72] J. Hopwood, C. R. Guarnieri, S. J. Whitehair, and J. J. Cuomo, J. Vac. Sci. Technol. A **11**, 147 (1993).

[73] M. Surendra, Plasma Sources Sci. Technol. **4**, 56 (1995).